AGU ADVANCING EARTH AND SPACE SCIENCE

Water Resources Research

RESEARCH ARTICLE
10.1029/2022WR033071

Determining the Flow State of Channels Under Vegetation With Airborne Lidar

J. W. Dillon[1], R. L. Lawrence[2], and K. D. Hammonds[1]

[1]Department of Civil Engineering, Montana State University, Bozeman, MT, USA, [2]Department of Land Resources and Environmental Sciences, Montana State University, Bozeman, MT, USA

Key Points:

- A reduction in the lidar return intensity of wet stream reaches under dense vegetation relative to dry channel reaches is statistically validated
- Optimal intensity thresholds for delineating wet from dry channel reaches obscured by vegetation are derived from probability density functions
- A classification workflow is presented to assign and map the flow state of obscured channel networks based on this novel phenomenon, with a median accuracy of 93.0%

Correspondence to:

J. W. Dillon and K. D. Hammonds,
james.dillon013@gmail.com;
kevin.hammonds@montana.edu

Citation:

Dillon, J. W., Lawrence, R. L., & Hammonds, K. D. (2023). Determining the flow state of channels under vegetation with airborne lidar. *Water Resources Research*, *59*, e2022WR033071. https://doi.org/10.1029/2022WR033071

Received 23 JUN 2022
Accepted 6 JUN 2023

Abstract Headwater channels are vital to ecological health, water quality, and watershed connectivity. However, the geographic extent and the temporal wetting and drying dynamics of headwater catchments are not thoroughly understood, primarily due to occlusive vegetation. Light Detection and Ranging (lidar) data can be utilized to address this knowledge gap. Airborne lidar is capable of penetrating vegetation and has been used as a spatial and spectral tool for water body delineation. In the work presented here we: (a) develop a novel means of normalizing lidar ground return intensity to allow for comparison across data sets; (b) demonstrate a statistically significant reduction in median return intensity of wet stream reaches under dense vegetation relative to dry channel reaches; and (c) leverage this reduction to create classified maps of wet and dry channel networks in densely vegetated drainages. Across four study basins spanning over 100 km^2 we observed an average reduction in median intensity of 41.7% and 72.2% for areas with and without dense vegetation, respectively. Optimal thresholds for delineating wet from dry stream reaches were determined using probability density functions. Resulting classified maps yielded overall accuracies ranging from 87.3% to 95.3% when compared to the National Hydrography Dataset via stratified random sampling. This study demonstrates that remote delineation of channel flow states in densely vegetated areas is possible, thus allowing for better consideration, designation, and conservation of headwater channels.

1. Introduction and Background

Wetted channel networks shrink and swell naturally, both seasonally, and in direct response to precipitation and snowmelt runoff events (Buttle et al., 2012; Hooshyar et al., 2015; Leopold & Miller, 1956; Uys & O'Keeffe, 1997). Flow regimes of these networks are altered by climate change, varying land-use, and diversion (Assendelft & van Meerveldt, 2019; Jacobson, 2004; Larned et al., 2010). Monitoring the temporal and spatial dynamics of channel flow states is vital in the fields of hydrology, geomorphology, ecology, and biochemistry (McDonough et al., 2011). For instance, observing wet versus dry reaches in a stream network can inform periodicity designations (i.e., perennial, intermittent, or ephemeral), as well as determinations of channel hydrological states (i.e., flowing, disjointed pools, or dry). Additionally, non-perennial streams provide biodiverse habitats (Meyer et al., 2007; Stehr & Branson, 1938) and migration corridors (R. Colvin et al., 2009; Erman & Leidy, 1975; Hartman & Brown, 1987), and also serve as biochemical reaction hotspots (McClain et al., 2003). Furthermore, an understanding of a watershed's hydrologic processes is intertwined with the temporal dynamics of its stream networks. Maps of wet channel networks help to improve surface-subsurface modeling (Camporese et al., 2010) and can be used for estimation of downstream flow rates (Godsey & Kirchner, 2014) and water quality (Romaní et al., 2006). Therefore, a high spatiotemporal resolution understanding of channel flow states is essential for models, management, and conservation practices. However, in many cases there are few available data on the wetting and drying dynamics of a drainage network. For example, stream gauges are often only located on relatively large, perennial rivers.

Remote sensing applications have contributed to a broader understanding of channel flow dynamics and periodicity by complementing conventional methods and addressing the limitations of discrete point measurements. For instance, near-infrared (NIR) satellite imagery produced by passive remote sensors has been used to map water bodies for decades, owing to the spectral signature of water (Work & Gilmer, 1976). At NIR wavelengths, water is highly absorptive relative to surrounding soil and vegetation, a contrast that is leveraged to differentiate surfaces in data products such as the Normalized Difference Water Index (NDWI) (McFeeters, 1996; Xu, 2006). However, mapping with passive remote sensing is generally restricted to large, open water bodies, limited by spatial resolution and a general inability to observe surfaces under the cover of forest vegetation (Assenfeldt

& van Meerveldt, 2019). Therefore, headwater catchments, where there is often dense vegetation cover and a prevalence of narrow and/or temporarily flowing channels, are often excluded. As a result, the geographic extent and temporal wetting dynamics of headwater streams, generally defined as the uppermost channels in a watershed, are not thoroughly understood (Hooshyar et al., 2015; Leopold, 1994; Meyer & Wallace, 2001; Nadeau & Rains, 2007). This is an unfortunate limitation, as headwater channels are the most abundant streams in both number and length in a drainage network (Horton, 1945; Leopold et al., 1964). Further, according to S. A. Colvin et al. (2019), they are thought to comprise 79% of total stream length in the U.S. Headwater streams are vital to ecological health, water quality, and watershed connectivity (Haigh et al., 1998; Wipfli et al., 2007).

Light Detection and Ranging (lidar) via airborne laser scanning (ALS) provides an opportunity to determine the flow status of channels in headwater catchments. As an active remote sensing system, lidar units emit rapid pulses of light (typically at a NIR wavelength) and record both the relative strength of backscattered signal after reflecting off a target, as well as the duration of travel. Each data point, or "return," has spatial coordinates (*X*, *Y*, and *Z*) and a return intensity value which provides a relative measure of target reflectance. Thus, lidar generates both a spatial and a spectral data product. Spatial lidar data are used extensively for topographic mapping, specifically toward the generation of Digital Elevation Models (DEMs). Lidar DEMs have been processed to delineate drainage networks (Lashermes et al., 2007; Orlandini et al., 2011; Passalacqua et al., 2010), hence using spatial, topographic data to outline systems of channels. In the context of this study, a drainage network determines where wet channels *could* be, but does not provide any information regarding which stream reaches are wet or dry. Furthermore, researchers have proven that lidar can achieve sufficient vegetation penetration to produce drainage network data products in certain forested areas. For example, James et al. (2007) and James and Hunt (2010) successfully circumvented canopy cover when mapping drainages in the Piedmont region of South Carolina, USA. Though part of the incoming radiation is intercepted by vegetation, enough energy is transmitted to provide spatial information on the ground beneath.

Complex hydrological pathways cannot by accurately portrayed with a sole reliance on topographic information, thus a variety of factors and information sources should be considered (Devito et al., 2005). For example, it has long been recognized that channel classification schemes that consider vegetation community structure and soil moisture patterns provide improved representation of water and sediment conveyance processes (Hack & Goodlett, 1960; Montgomery, 1999). More recently, measurements of surface roughness and texture derived from lidar have proven useful for detecting specific stream channel components including large woody debris (Abalharth et al., 2015). This study builds on the recent work utilizing lidar intensity data to improve drainage network maps by leveraging spectral lidar intensity data to detect the presence of water in channels, much like passive NIR satellite imagery. As mentioned above, water is relatively absorptive at the NIR wavelengths commonly used in lidar ALS systems. Because of this absorption, related studies found that water bodies are characterized by low return intensity (Brzank et al., 2008; Höfle et al., 2009), as more of the incoming radiation is absorbed by water relative to adjacent land areas. The resulting regions of distinctly low intensity have been shown to effectively outline water surfaces and inundated areas (Antonarakis et al., 2008; Lang & McCarty, 2009). Similarly, interactions between NIR lidar and water tend to yield laser shot dropouts, where the reflected signal is so weak that it does not generate a return. The resulting regions of low point density can also be used to delineate water body boundaries (Worstell et al., 2014). However, most studies have focused on large and/or open water bodies, rather than explicitly addressing the problem of small channels under dense vegetation.

Forested areas present a challenge for delineating water bodies with lidar intensity. This is because vegetation occlusion tends to yield ground returns with lower intensity than those of open ground, similar to the low intensity of water targets. Figure 1 illustrates a simplified schematic of four possible lidar return scenarios, and demonstrates this problem. Figures 1a and 1b depict the case of an open area without any obstruction from vegetation, where the lidar beam encounters dry ground and water, respectively. As discussed above, water is absorptive in the NIR spectral region, and so the return intensity from water is markedly lower. In the second row, dry ground and water are obscured by vegetation (Figures 1c and 1d, respectively). Vegetation scattering results in multiple returns from a single pulse that can be used to create maps of vegetation height. However, because only a portion of the outgoing pulse reaches the ground, less energy is available for scattering at the ground level, resulting in distinctly lower ground return intensity relative to open areas, even when dry ground is encountered (e.g., Figure 1a vs. 1c). This makes it difficult to rely solely on the spatial distribution of return intensity as an indicator of water when vegetation is present, as low-intensity returns from the scenarios in Figures 1b–1d could easily be conflated.

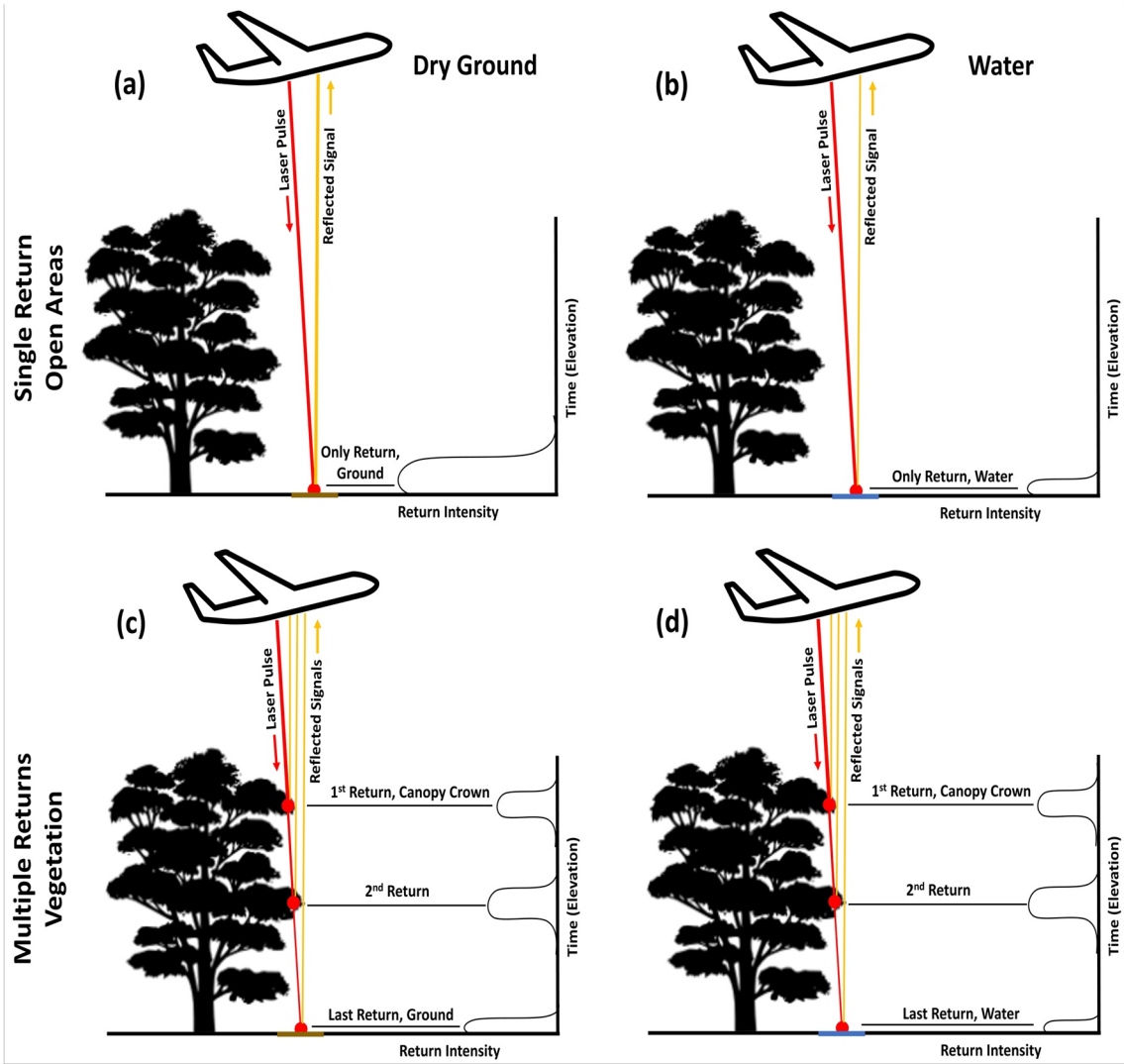

Figure 1. Simplified schematic of four lidar scattering scenarios. Single returns in an open area from dry ground and water (a and b, respectively) are compared to multiple returns from vegetation scattering (c and d) with the same ground cover.

Previous researchers have attempted to circumvent the issue of vegetation obscuring airborne lidar. In Hooshyar et al. (2015), a study focused on headwater catchments with considerable vegetation, the researchers actively masked nearby dense vegetation in their intensity maps to prevent the erroneous classification of wet surfaces. As a result, they acknowledged that their method is limited to partially covered channels. In the case of stream channels largely occluded by vegetation, however, this tactic would result in masking of the water returns we seek to map. Thus, when dense vegetation is prevalent this method becomes impracticable. Figure 2 illustrates this limitation. The left column demonstrates successful masking on a sparsely covered stream, while the more densely forested area in the right column contains a well-hidden channel which complicates masking. To begin, National Hydrography Dataset (NHD) flowlines confirm the presence of perennial channels at two different locations (Figures 2a and 2b). The presence of low-intensity noise from vegetated areas around the channels is evident in the raw intensity maps for both areas (Figures 2c and 2d). Using vegetation maps (Figures 2e and 2f), pixels coincident with dense vegetation are excluded, resulting in masked ground intensity maps (Figures 2g and 2h). Successful masking on the larger channel in the left column allows for easy delineation. This is not the case in the narrower, more occluded perennial channel in the right column. Because much of the channel is under canopy cover, 89% of the pixels coincident with the channel are caught in the filter and masked, eliminating their intensity data.

10.1029/2022WR033071

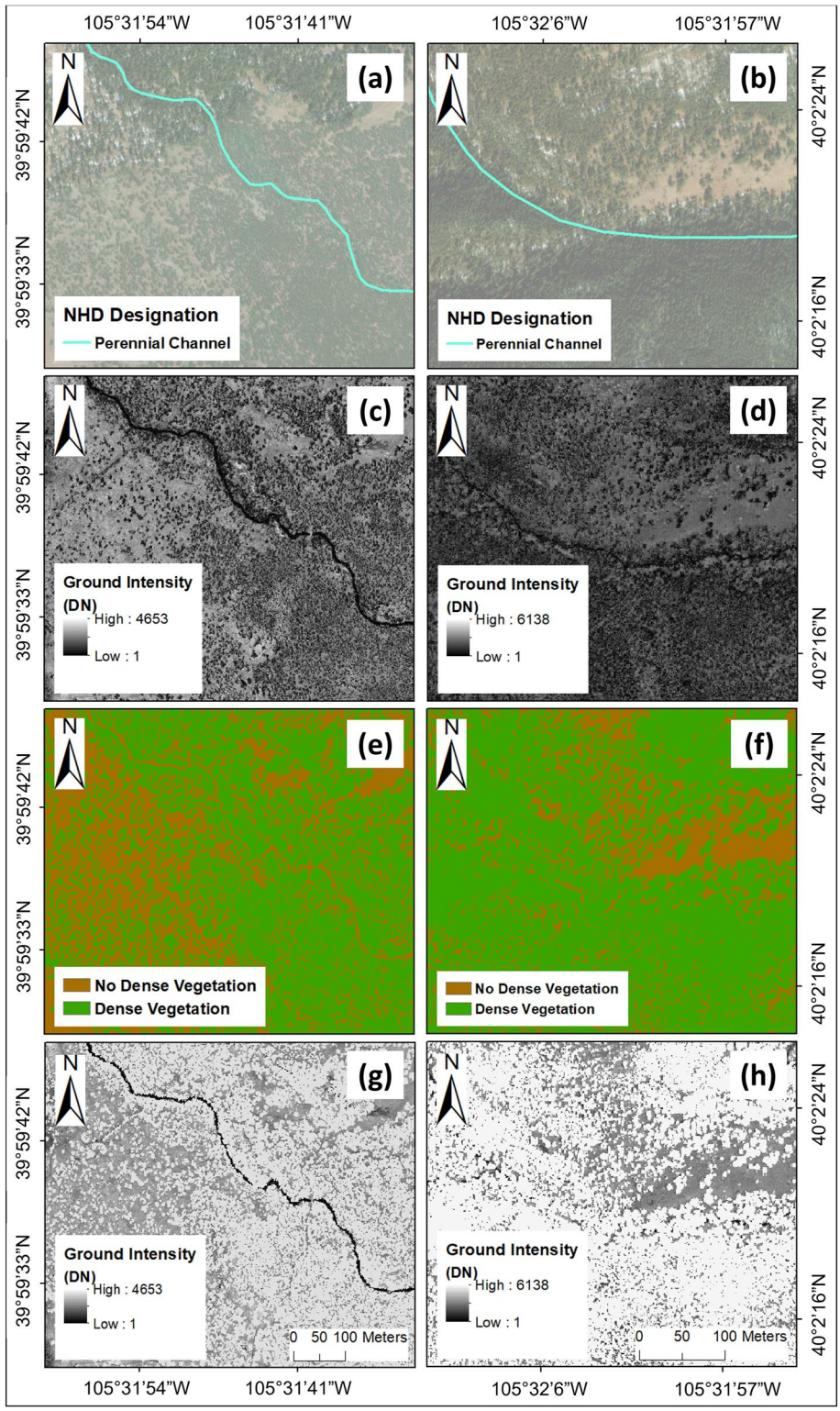

Figure 2. Pilot study results from the study area with aerial imagery (a and b), raw ground return intensity maps (c and d), the extent of dense vegetation (e and f) and resulting ground intensity maps after masking densely vegetated areas (g and h). The left column demonstrates successful masking allowing for delineation of a larger, sparsely vegetated channel, while the right column illustrates how vegetation masking is impracticable on smaller, occluded channels. Dense vegetation refers to locations where the elevation difference between the top of the forest canopy and the ground is greater than 2 m, following Hooshyar et al. (2015), while no dense vegetation essentially implies an open area.

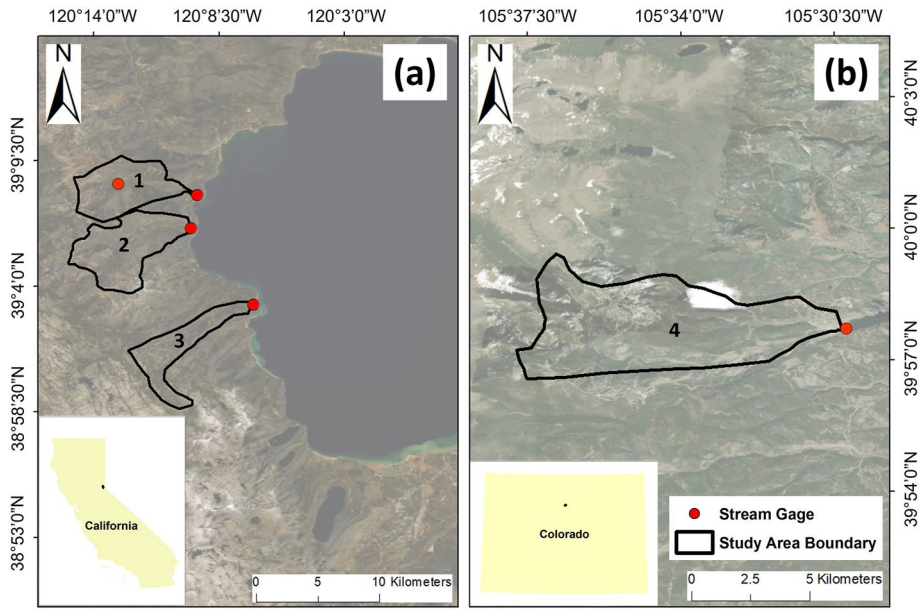

Figure 3. Map of study basin locations.

In summary, the capacity of lidar to map drainage networks under dense vegetation using spatial data has been demonstrated, and spectral lidar intensity data have been used to outline water bodies. However, determining which channels are wet versus dry in headwater catchments continues to present a challenge, particularly in forested regions or areas with dense riparian vegetation. Though airborne lidar can penetrate canopy, the use of lidar intensity data to locate wetted channel networks under vegetation is an unvalidated method. In the work presented here, we attempt to address this knowledge gap by presenting a novel method for classifying wet and dry stream reaches in forested areas. Intuitively we note that, in the case of identical vegetation conditions, liquid water under canopy should produce a lower return intensity signal when compared to dry ground, due to its lower NIR reflectance. Therefore, *we hypothesize that a quantifiable reduction in ground return intensity exists when a lidar signal encounters both dense vegetation and liquid water at the ground surface, relative to vegetation with dry ground beneath*. To explore this prospect, we selected study basins in California and Colorado with lidar, hydrometric data, and dense riparian forests. We first use spatial lidar data to delineate drainage networks and identify the presence of occlusive vegetation. Next, frequency distributions of ground return intensity under dense vegetation are evaluated to statistically compare wet versus dry occluded channels. Per our hypothesis, an intensity reduction in occluded wet channels relative to dry channels is expected. A quantifiable intensity reduction can then be leveraged to create a classified map product depicting wetted channel connectivity in headwater catchments with dense vegetation. Lidar-derived maps of wet channel networks could be used to determine headwater stream periodicity in regions lacking reference data, to observe intraannual wetting and drying dynamics at high spatiotemporal resolution, or to detect changes in stream permanence due to changing climate and land use. Specifically, there are no existing approaches for broad scale tracking of the potential expansion of intermittent and ephemeral channel extent in response to changes in frequency and intensity of drought.

2. Study Basins and Data

2.1. Study Basins

Three study areas (Basins 1–3) along the western shore of Lake Tahoe, CA, also utilized by Hooshyar et al. (2015), are revisited (Figure 3a). These basins benefit from overlapping lidar and hydrograph data. The boundaries of Basins 1–3 are delineations of complete catchments, each with a United States Geological Survey (USGS) stream gage at the outlet. Basin 1 features an additional gage along Ward Creek several kilometers upstream of Lake Tahoe. Basin 4 includes most of the Middle Boulder Creek catchment, except for an area lacking lidar data availability (Figure 3b). Basin 4 also drains to a continuous stream gage, managed by the Colorado Department of Water Resources, before flowing into the Barker Meadow Reservoir. Relevant historic hydrometric statistics and

Table 1
Study Basin Statistics

Site #	Primary perennial stream	Area (km^2)	Lidar acquisition date(s), 2010	Gage (#)	Mean acquisition flow rate (m^3/s)	30-day low flow rate (m^3/s)	Mean annual flow rate (m^3/s)	Peak flow rate (m^3/s)
1	Ward creek	23.1	14 August	USGS 10336676	0.06 (8.3%)	0.02 (2.8%)	0.68 (93.7%)	8.63 (1189.0%)
				USGS 10336674	0.07 (15.3%)	0.03 (6.6%)	0.40 (87.5%)	5.26 (1151.0%)
2	Blackwood creek	28.4	20–23 August	USGS 10336660	0.11 (11.0%)	0.04 (4.0%)	0.89 (88.6%)	10.61 (1056.8%)
3	General creek	18.2	20–23 August	USGS 10336645	0.02 (4.3%)	0.02 (4.3%)	0.45 (97.0%)	6.11 (1316.8%)
4	Middle boulder creek	31.9	20–21 May 21–26 August	CO DWR BOCMIDCO	2.26 (138.9%) 0.82 (50.4%)	0.09 (5.5%)	1.44 (88.5%)	15.48 (951.4%)

Note. Acquisition flow rates refer to the mean measured flow at the stream gages during periods of lidar scanning. Mean annual, 30-day low, and peak flow rate metrics represent the 2010 water year for each gage. Values are also presented as a percentage of the long-term mean annual discharge (% LT MAD) consistent with Tennant (1976) where flows >200% represent flushing flows, and flows <10% represent severe degradation for fish resources.

flow at the time of lidar acquisitions were obtained for these stations. Furthermore, Basin 4 lidar data were acquired in May and August, allowing for a temporal comparison. The western side of Lake Tahoe receives a mean annual precipitation of 140 cm, while Nederland, CO on the eastern end of Basin 4 reports 72 cm. Precipitation at all basins primarily falls between November and May, with most runoff occurring during spring snowmelt, typically peaking in May and June. Basins are largely covered by dense, intact forest, with minimal disruption from human development and urbanization. Study basin areas ranged from 18.2 to 31.9 km^2 (Table 1).

2.2. Data

Lidar data for Basins 1–3 were acquired from the Lake Tahoe Basin LiDAR data set, collected by Watershed Sciences, Inc. in conjunction with the Tahoe Regional Planning Agency. Data for Basin 4 was from the Boulder Creek Critical Zone Observatory LiDAR Survey collected by the National Center for Airborne Laser Mapping (NCALM). All data were accessed through the Open Topography public repository. Researchers at Basins 1–3 utilized a 1,064 nm laser, while Basin 4 researchers used 1,047 nm, both NIR wavelengths. Other relevant statistics from the data collection campaigns are listed in Table A1. To reiterate, each lidar return has spatial coordinates (*X*, *Y*, and *Z*) and a range-calibrated return intensity value. A single pulse can generate multiple returns when vegetation is present, as previously illustrated in Figures 1c and 1d. This allows for elevation and intensity data to be segregated via return number, such that sub-data sets can be determined for both the ground and canopy crown layers.

In the Tahoe area, lidar data at Basins 1 and 2 were collected while discharge approached 30-day low flow rates, while Basin 3 lidar data were collected at the 30-day low flow rate (Figure 4a). Therefore, scans coincided with flows expected to cause dry channels in some locations. Weather data procured from the National Climate Data Center (NCDC) revealed no precipitation during lidar data collection at the nearest station in Tahoe City, CA. Wet and dry season lidar data are available for Basin 4, as aerial scanning was conducted in both May and August of 2010 (Table 1). Both outings coincided with transitional periods (Figure 4b). May data collection in Basin 4 took place after the watershed had surpassed the mean annual flow rate (139% LT MAD), 17 days before peak flows were reached. In contrast, the August data collection in Basin 4 occurred during hydrograph recession, with flows at 50% LT MAD. Hereafter, the May and August lidar data sets for Basin 4 will be referred to as Basins 4M and 4A, respectively. Once again, weather data provided by the NCDC showed no precipitation at the Nederland, CO station during either data collection campaign.

The NHD, accessed via the USGS National Map, was used as reference data. The NHD is considered to be the most comprehensive and up-to-date hydrography data set for the United States, used extensively from local to national scales (Hafen et al., 2020; Nadeau & Rains, 2007; Simley, 2006). The positions of NHD flowline features, including streams, were manually surveyed by USGS field crews using the standards of the day for Digital Line Graphs (https://pubs.usgs.gov/circ/1984/0895g/report.pdf). During topographic inspection, stream periodicity classifications (i.e., perennial, intermittent, or ephemeral) were determined based on several factors, including previous observations, feedback from local residents, water containment, soil type, and vegetation at the time of the site visit (Personal communication from D. Anderson, USGS Hydrography Program, to J. Dillon, 17 November 2022). Periodicity determinations were meant to represent stream permanence across a normal range of climactic conditions (Hafen et al., 2020). Furthermore, many NHD flowline geometries and periodicities have since been updated by partnering state agencies as part of a stewardship program, leveraging local knowledge. All flowlines in Basins 1–3 were updated between 2012 and 2016, while flowlines in Basin 4 were recompiled in 2012. Thus, position and periodicity determinations for streams in all study basins were recently assigned by state agencies based on field observations. The USGS defines perennial streams as those which normally have water in their channel year-round, except for infrequent periods of severe drought (https://nhd.usgs.gov/userguide.html). Intermittent streams tend to flow seasonally, only when receiving water from rainfall runoff, springs, or other surface sources such as snowmelt. Last, ephemeral streams flow only in direct response to precipitation. They receive little to no water from springs, snowmelt, or other sources,

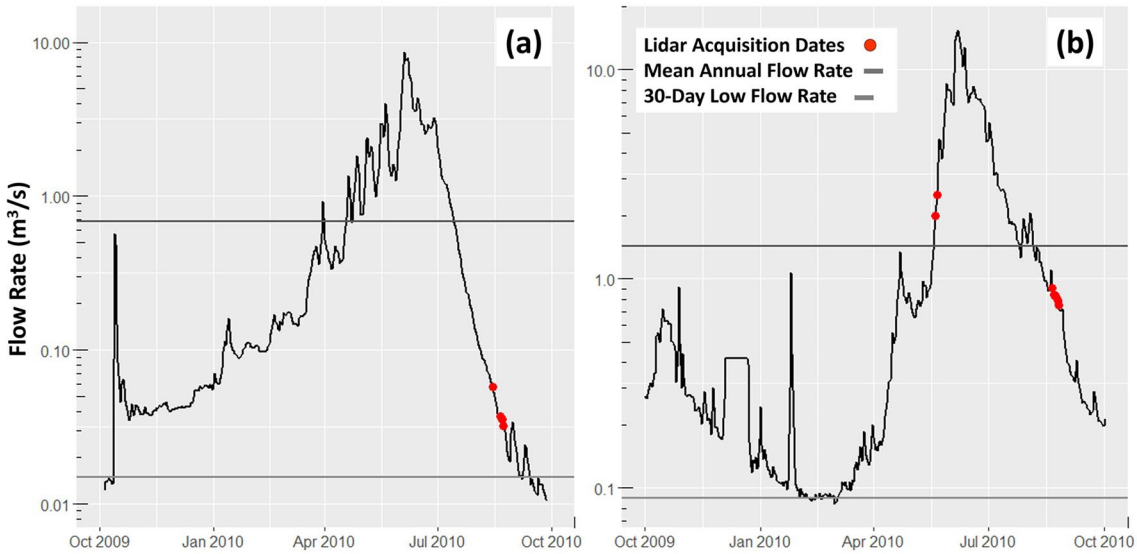

Figure 4. Hydrographs and lidar acquisition dates for Basin 1 (a) and Basin 4 (b). The hydrograph for Basin 1 uses data from the downstream gage (# 10336676) at the mouth of Ward Creek. The Basin 1 hydrograph is representative of Basins 2 and 3 (as well as the upstream gage at Basin 1), and includes lidar acquisition dates for all Lake Tahoe study basins. Horizontal lines depict the mean annual flow and the 30-day low flow rate for the 2010 water year.

and their channels remain above the water table at all times. Based on these definitions and the data in Table 1 and Figure 4, the following classification rules were created for reference data:

Basins 1–3, 4A

- Perennial streams were assumed to be wet
- Intermittent and ephemeral reaches were presumed dry

Basin 4M

- Perennial streams were assumed to be wet
- Intermittent reaches were presumed wet; at 139% LT MAD, flows were likely high enough to activate intermittent channels, with snowmelt runoff driving the exponential rise of the hydrograph
- Ephemeral streams were still assumed to be dry, as flows at only 15% of peak discharge likely were not high enough to activate ephemeral channels

3. Analysis and Methodology

Water surfaces are characterized by low return intensity relative to dry ground, a spectral signature that is used to map wet channels via an intensity threshold (Antonarakis et al., 2008; Brzank et al., 2008; Höfle et al., 2009). However, dense vegetation generates low-intensity noise that complicates water body classification. We hypothesized that, even when under dense vegetation, wet stream reaches will produce a significantly lower return intensity relative to dry ground under vegetation. In the work presented here we statistically validate that such a reduction is consistently quantifiable and reproduceable. Further we leverage this phenomenon, along with spatial lidar data, to wet from dry channels in densely vegetated areas. Our analyses consisted of four major tasks: (a) development of relevant map layers, (b) normalization of intensity data, (c) statistical analysis and (d) generation of classified maps. All work was performed using ESRI's ArcMap 10.7.1 (ESRI, 2020) and the statistical programming software R (R Core Team, 2022).

3.1. Map Layer Development

Several pertinent map layers were produced from raw lidar data (Figure 5). To begin, subgroups of ground returns, as classified by the data collectors (Watershed Sciences, Inc. and NCALM; Section 2.2) using TerraSolid's TerraScan software, were separated from the remainder of the lidar data set. The intensity values from ground

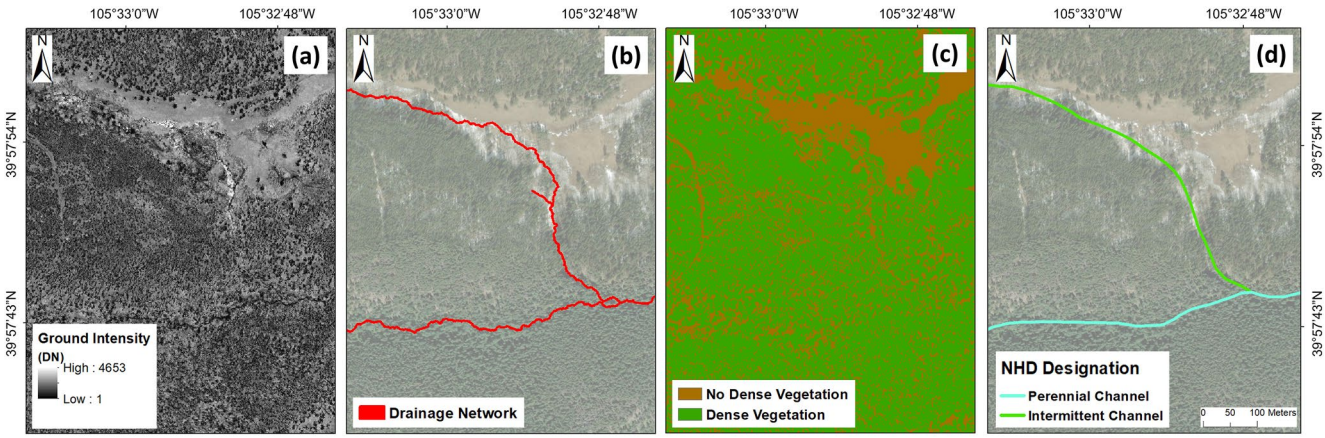

Figure 5. Core map layers to be used in the following analyses: ground intensity (a), drainage network delineation (b), binarized vegetation (c), and National Hydrography Dataset channel designations as reference data (d). The perennial channel shown is North Beaver Creek in Basin 4.

returns were interpolated to create a map of ground return intensity (Figure 5a). Similarly, elevation values from ground returns were interpolated to yield a DEM. Using the workflow of Omran et al. (2016), the DEMs were processed to produce maps of drainage networks (Figure 5b). Next, first returns and only returns were separated, and this subgroup's elevation data were interpolated to produce a Digital Surface Model (DSM). The DSM is identical to the DEM when vegetation is absent but represents the elevation of the top of the canopy when it is present. Subtracting the DEM from the DSM results in a map of canopy height. This canopy height model is then binarized; pixels with a vegetation height value greater than 2 m were categorized as "dense vegetation," while all other pixels were classified as "no dense vegetation" (Figure 5c), following Hooshyar et al. (2015). The spatial resolution of all maps was 1 m. Last, maps of NHD stream classifications served as reference data (Figure 5d).

3.2. Intensity Normalization

To compare values across different basins and data sets, we normalized all intensity maps using a common land cover feature. Given our interest in canopy obstruction, we examined the average intensity of dry pixels under dense vegetation. For each data set, a series of overlays were used to isolate ground intensity pixels coincident with dense vegetation and outside of the drainage network. The mean values of these intensity subsets were calculated, and termed $\overline{I}_{ND,V}$; the mean intensity of pixels both outside the drainage network, or non-drainage (ND), and under dense vegetation (V). This value was used as the normalizing factor for each data set via Equation 1:

$$I^{nor} = \frac{I}{\overline{I}_{ND,V}} \tag{1}$$

where I is the raw intensity and I^{nor} is the unitless normalized result for a given pixel. Hereafter, the superscript "nor" implies that an intensity value has been normalized, while subscripts denote the data subsets that the value is associated with. By applying Equation 1, we normalized by the *mean effect of canopy occlusion* for a given basin/data set, allowing for comparison across data sets spatially and temporally. For example, a value of I^{nor} less than 1 denotes a pixel with lower intensity than the average value of dry ground under dense vegetation.

3.3. Statistical Analysis

The goal of statistical analysis was to investigate our hypothesis: that a significant reduction in return intensity occurs in wet channel pixels relative to their dry channel counterparts, *even when under dense vegetation*. Further, we sought to determine the optimal thresholds of normalized intensity (I^{nor}) to map wet channels within a drainage network, whether open or occluded by dense vegetation.

For each data set, pixel values of I^{nor} were first divided into four subgroups: (a) wet channels/dense vegetation, (b) dry channels/dense vegetation, (c) wet channels/no dense vegetation, and (d) dry channels/no dense vegetation. Figure 6 describes this segregation workflow; recall subscripts correspond to data set subgroups. To begin, maps

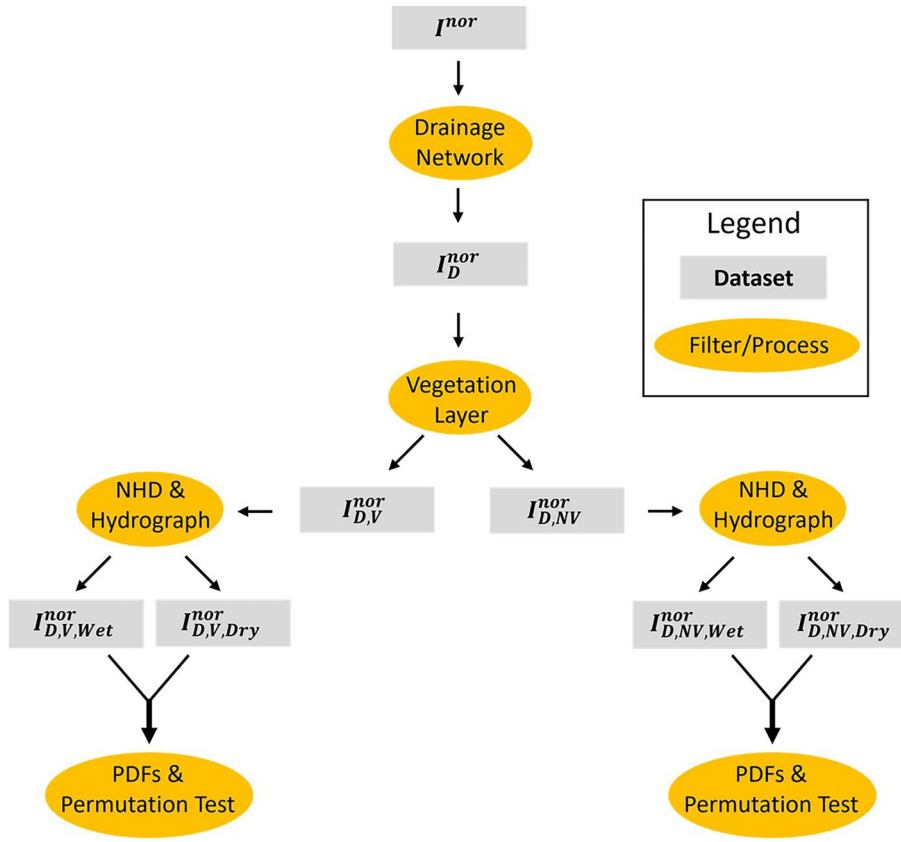

Figure 6. Workflow for subdividing pixels of Normalized Intensity (I^{nor}) maps.

of I^{nor} were truncated to only include pixels within the drainage network (D), termed I_D^{nor}. Next, I_D^{nor} values were further sorted by the presence (V) or absence (NV) of dense vegetation ($I_{D,V}^{nor}$ and $I_{D,NV}^{nor}$, respectively). Last, pixels were separated into bins coincident with wet streams versus dry channels, using the description and reference data rules in Section 2.2. For instance, following the convention discussed above, $I_{D,V,Wet}^{nor}$ would refer to the normalized intensity of pixels within the drainage network (D), under dense vegetation (V), and coincident with a known wet stream segment (Wet) as determined by the NHD and hydrograph data. To reiterate, NHD-designated perennial channels were assumed wet across all data sets, and all other channels presumed dry with the exception of intermittent streams in data set 4M (Section 2.2).

For each data set, a pair of significance tests were conducted to evaluate the difference in I^{nor} distributions between wet and dry channel pixels; one for the case of dense vegetation and the other for no dense vegetation. In other words, $I_{D,V,Wet}^{nor}$ was compared to $I_{D,V,Dry}^{nor}$, while $I_{D,NV,Wet}^{nor}$ was compared to $I_{D,NV,Wet}^{nor}$ (Figure 6). To restate our hypothesis, we expect that $I_{D,V,Wet}^{nor}$ and $I_{D,NV,Wet}^{nor}$ values will be significantly lower than their "Dry" counterparts based on previous work and radiative transfer theory. When comparing median values, our hypotheses can be summarized as follows:

$$H_0 : M\left(I_{D,V,Wet}^{nor}\right) = M(I_{D,V,Dry}^{nor}) \text{ and } M\left(I_{D,NV,Wet}^{nor}\right) = M(I_{D,NV,Dry}^{nor})$$

$$H_A : M\left(I_{D,V,Wet}^{nor}\right) < M(I_{D,V,Dry}^{nor}) \text{ and } M\left(I_{D,NV,Wet}^{nor}\right) < M(I_{D,NV,Dry}^{nor}); \alpha = 0.05$$

Each of the four subgroups were randomly sampled with replacement to a sample size of 3,198 pixels, the size of the smallest data set. Doing so ensured equal sample sizes and addressed the rather large range in pixel count values across data sets. A one-sided permutation test was preferred to a traditional t–test, as assumptions of equal variance and normality appeared to be violated in some cases. Further, the permutation test was conducted to compare median I^{nor} values between data sets, rather than means. Although a comparison of means is a typical default, a preliminary examination of intensity distributions revealed large outliers in some data sets. As outliers

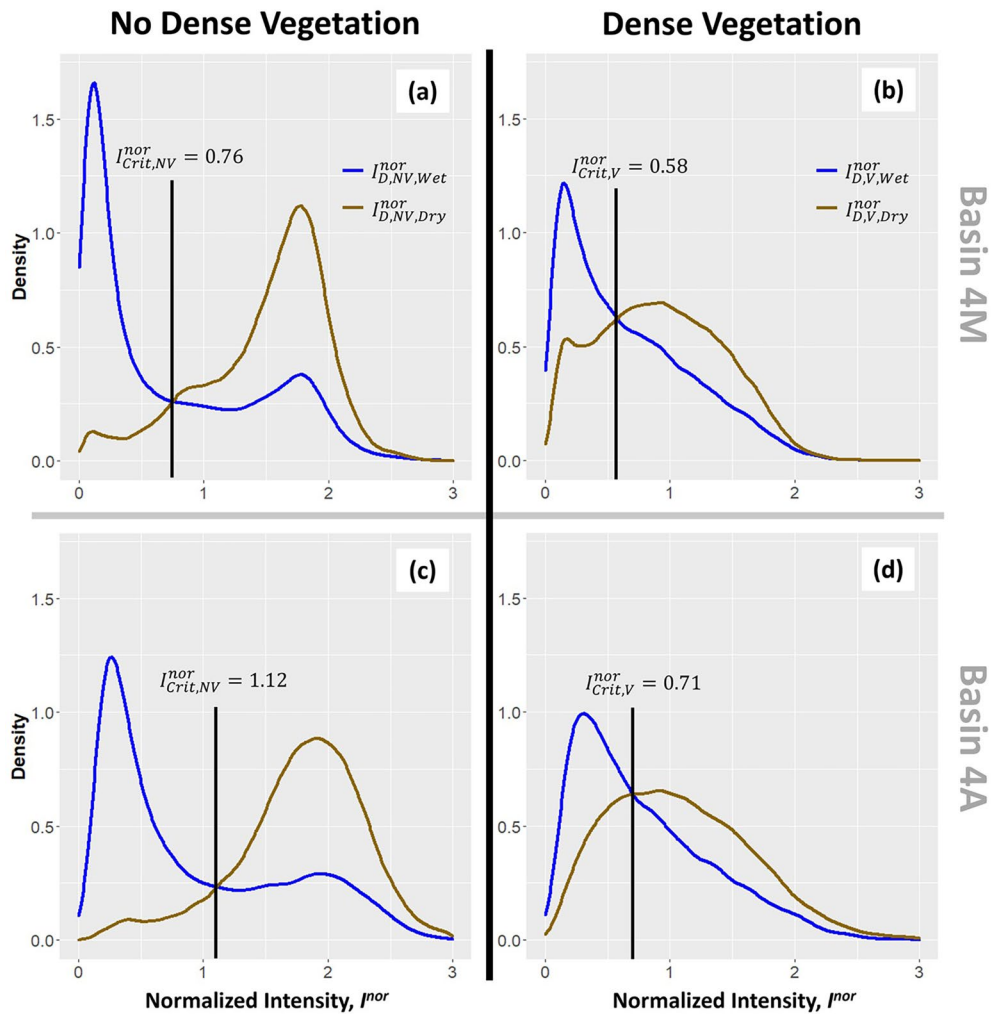

Figure 7. Example probability density functions to contrast intensity distributions of wet and dry pixels. The distributions shown are from data sets 4M and 4A. Vertical black lines at distribution intersections represent critical thresholds for delineating wet from dry streams for each data set and vegetation state.

can produce mean values that poorly represent the overall distribution, medians were analyzed to mitigate the presence of outliers. Resulting p-values represent the probability that a difference in median I^{nor} values between wet and dry channel pixels is due to random variation. Therefore, low p-values would provide evidence for our hypothesis. P-values for each comparison were recorded, as well as median and standard deviation information for each data set.

Last, frequency analyses were performed on intensity maps to create probability density functions (PDFs), used to visually contrast the distributions of wet versus dry stream channels for both the case of dense vegetation and no dense vegetation. For each data set and vegetation state, the intersection of wet and dry PDFs was deemed the optimal threshold to delineate wet from dry pixels in a drainage network (Figure 7). These optimal cutoff points, or critical thresholds, were termed $I^{nor}_{Crit,V}$ and $I^{nor}_{Crit,NV}$, ideal delineation values for dense vegetation (V) and no dense vegetation (NV), respectively.

3.4. Wet Channel Classification

The statistical analyses presented in Section 3.3, specifically values of $I^{nor}_{Crit,V}$ and $I^{nor}_{Crit,NV}$, were used to produce a classified map product. Each pixel in the drainage network was classified as wet or dry. An outline of this workflow is presented in Figure 8. Once again, maps of I^{nor} (Figure 8a) were truncated using the drainage network

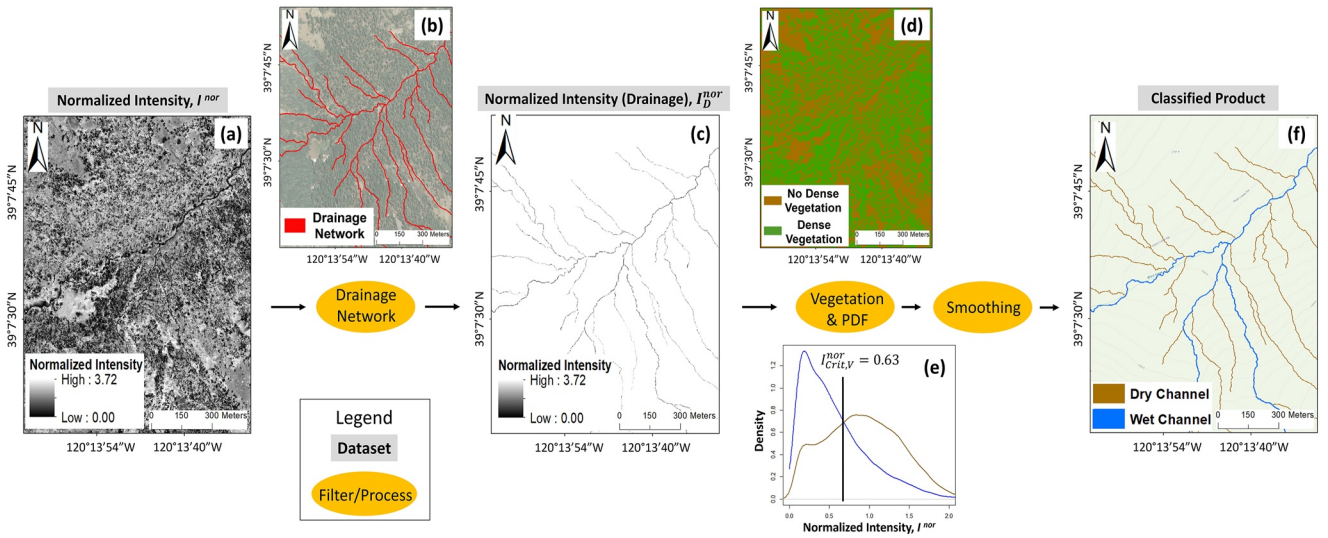

Figure 8. Demonstration of classification workflow. A normalized ground intensity map, I^{nor} (a) is trimmed by the coincident drainage network (b) to only include pixels within the network, I_D^{nor} (c). Using a binarized vegetation map (d) and a probability density function analysis (e), a classified product is produced (f). The channel shown is Ward Creek in Basin 1.

(Figure 8b) to include only pixels within the network, I_D^{nor} (Figure 8c). Next, depending on whether a drainage pixel was coincident with dense vegetation (Figure 8d), the appropriate critical threshold from the PDF (Figure 8e) was applied to classify pixels as wet or dry. In the example presented, drainage pixels under dense canopy with an I_D^{nor} value less than 0.63 would be classified as wet, and vice versa. Last, following previous models (e.g., Hooshyar et al., 2015), a final smoothing step was performed to minimize the influence of isolated misclassified pixels on overall accuracy. All pixels in a given stream link were reclassified to the majority assignment, resulting in the final data product (Figure 8f). A stream link is defined as a section of channel between two successive junctions.

The accuracy of each classified map was assessed against the NHD with a stratified random sample of 300 points. Following Foody (2009), a minimum total sample size of 200 points was determined based on an expected accuracy of 85% and allowable sampling error of 5%. This value was then increased to 300 points to ensure a minimum of 50 points per each stratum, considering the popular heuristic metric dating back to Hay (1979). Confusion matrices of the form depicted in Figure 9 were produced to display classification results. Perhaps the most widely utilized accuracy assessment approach in remote sensing, a confusion matrix is a table used to clearly and concisely summarize the performance of a classification algorithm (Foody, 2002). For example, in Basins 1–3 where low-flow conditions were present at the time of lidar data acquisition, it was assumed that only perennial channels were flowing (see description and reference data rules in Section 2.2). Therefore, reaches classified as wet that were coincident with NHD-designated perennial channels would qualify as a TP, while wet classifications on all other channels were FPs. Accuracy was calculated with Equation 2 from the seminal work of Story and Congalton (1986). Furthermore, modeled values of total wet channel length from classified maps were compared to those of the NHD.

		Modeled	
		Wet	*Dry*
Reference	*Wet*	TP	FN
	Dry	FP	TN

Figure 9. Example confusion matrix. In this case true positives (TPs) refer to the number of wet pixels correctly classified as wet, false negatives (FNs) to the number of pixels classified as dry that were actually wet, and so on. Reference designations of wet and dry regions were based off of the National Hydrography Dataset according to the rules in Section 2.2.

$$\text{Accuracy, } A = \frac{TP + TN}{TP + TN + FP + FN} \quad (2)$$

4. Results

4.1. Summary of Basic Statistics and Significance Testing

Frequency distributions for samples of I_D^{nor} had significantly lower median values in wet channels when compared to dry channels (Table 2). A reduction was observed both when dense vegetation was present (a novel result) and in its absence (an expected result). Under dense vegetation the average reduction in median $I_{D,V}^{nor}$ values was 41.7%, compared to a 72.2% intensity

Table 2
Probability Density Function and Classification Results

Data set	Median (sd) $I^{nor}_{D,V,Wet}$	$I^{nor}_{Crit,V}$	Median (sd) $I^{nor}_{D,V,Dry}$	Median (sd) $I^{nor}_{D,NV,Wet}$	$I^{nor}_{Crit,NV}$	Median (sd) $I^{nor}_{D,NV,Dry}$	Modeled wetted length (km)
1	0.41 (0.59)*	0.63	0.97 (0.68)	0.21 (0.61)*	0.75	1.52 (0.61)	19.0
2	0.43 (0.56)*	0.53	0.76 (0.59)	0.27 (0.61)*	0.76	1.46 (0.54)	23.7
3	0.76 (0.55)*	0.92	1.10 (0.56)	0.75 (0.60)*	1.14	1.55 (0.46)	22.7
4M	0.53 (0.70)*	0.58	0.89 (1.31)	0.40 (0.81)*	0.76	1.62 (1.48)	32.0
4A	0.66 (0.78)*	0.71	1.03 (0.61)	0.62 (1.77)*	1.12	1.84 (1.22)	29.5

Note. Asterisks (*) adjacent to wet intensity statistics denote statistically significant reductions relative to dry pixels at $\alpha = 0.05$.

reduction in open areas, $I^{nor}_{D,NV}$. In each case, one-sided permutation tests produced values of $p < 0.001$ across all data sets, and thus intensity reductions in wet relative to dry channels were highly significant. In other words, the probability that these reductions were caused by random variation is very low. Therefore, our primary hypothesis was confirmed: even when dense vegetation created low-intensity noise in dry ground returns, *the median intensity of occluded wet channels was quantifiably lower.*

4.2. Classified Network Maps

Reference wet channel lengths from the NHD are compared to modeled values from classified maps in Figure 10. Modeled data was in reasonably good agreement with the NHD, although a tendency to underestimate wet channel length is observed, particularly in data set 4M. Classified maps for Basins 1–3 and their coincident NHD designations are illustrated in Figure 11, along with Accuracy, *A* values from stratified random sampling. The same can be found for Basin 4 in Figure 12, with a temporal comparison between data sets 4M and 4A. Accuracy ranged from 87.3% to 95.4% with a median of 93.0%. In Basins 1–3, ephemeral and undesignated channels were almost entirely rejected from the wet channel classification, and much of the perennial channel length was correctly classified. These basins performed slightly better than 4M and 4A, with a minimum accuracy of 93.0% ranging to 95.4%. In both 4M and 4A most perennial channels were correctly designated as wet and ephemeral as dry. Further, all intermittent reaches were classified as dry in 4A, while several intermittent stretches were classified as wet channels in 4M, as we would expect. Therefore, True Negative (TN) classifications were abundant in 4M and 4A, while False Positives (FPs) were almost nonexistent. False Negatives (FNs) were the primary source of error in each case, consistent with the low bias seen in Figure 10.

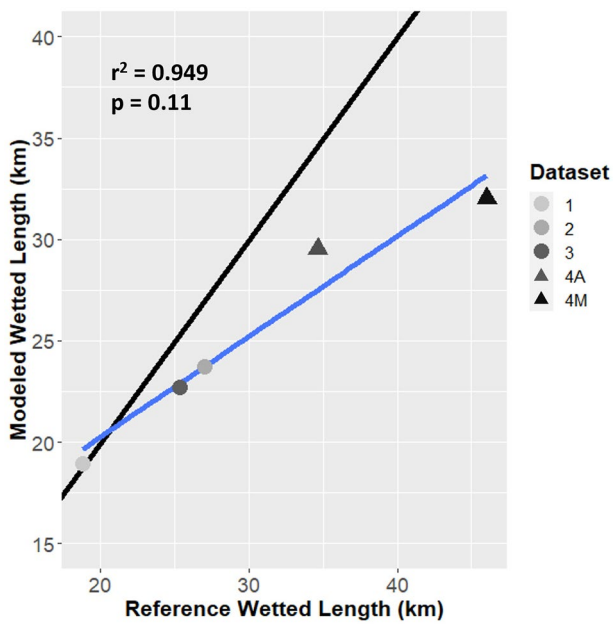

Figure 10. Modeled wet stream length values from the classification workflow compared to National Hydrography Dataset data. The blue line is a linear best fit while a 1:1 reference line is in black. Values are colored by data set, while shapes correspond to general locations. Hence Tahoe Basins 1–3 are circular and both data sets for Basin 4 in Colorado are triangular.

We observe that a portion of classification error can be attributed to improper network delineation, rather than a failure of our ground intensity reduction hypothesis. The delineation workflow of Omran et al. (2016) was primarily selected for drainage network delineation due to its demonstrated capability, ArcMap compatibility, and computational efficiency. Though resulting drainage network maps exhibited good agreement with NHD flowlines, some artifacts were visibly observable, namely due to interference from roads. For example, the perennial channel in the northeast quadrant of Figure 12 (North Beaver Creek, red rectangle) was sporadically misclassified as dry in both 4M and 4A, despite being a relatively large, continuously wetted stream. In these cases, the drainage network maps occasionally deviated from the actual stream channel. Thus, intensity data were incongruent with spatial network

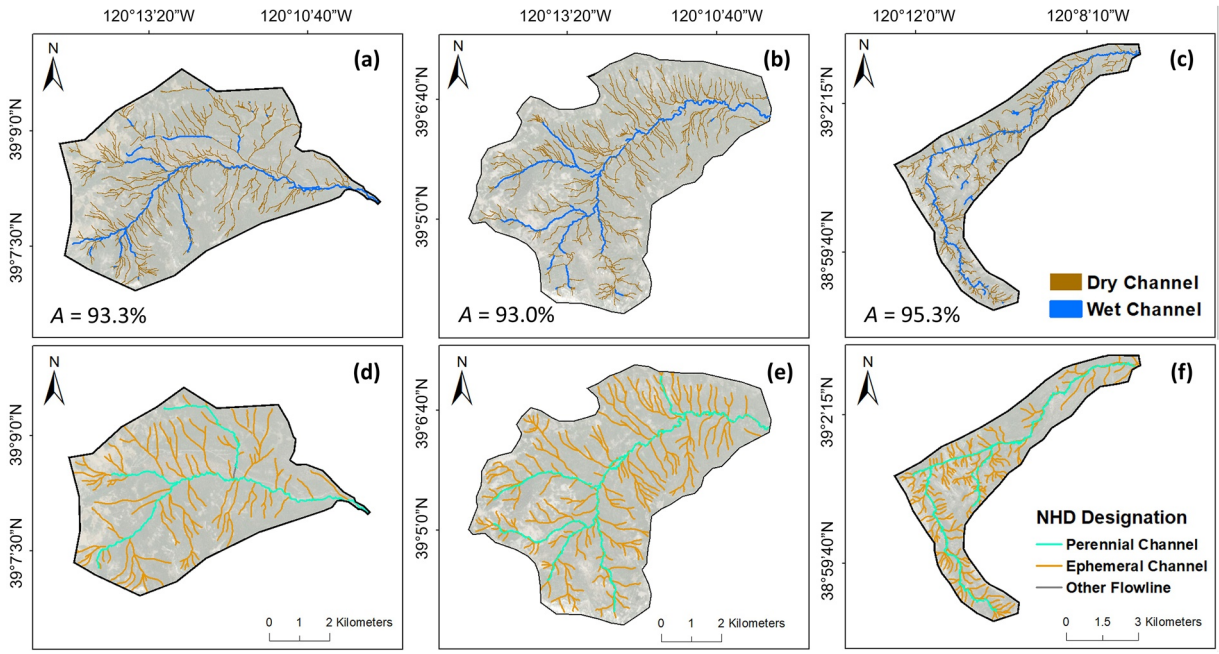

Figure 11. Classified maps depicting the extent of modeled wet and dry channel lengths (a–c) compared to NHD channel designations (d–f) for Basins 1–3 overlaid on aerial imagery.

delineations, and misclassification ensued. As a result, we note the importance of site-specific network segregation prior to integrating lidar intensity data.

5. Discussion

In the work presented here we (a) developed a novel means of normalizing lidar ground return intensity to allow for comparison across data sets, (b) demonstrated a statistically significant reduction in median return intensity of wet channels under dense vegetation relative to dry channels, and (c) leveraged this reduction to create maps of wet channel networks in densely vegetated drainages. In practice, any representative area where hydrologic conditions are known could be used to calibrate, or train the model by finding the optimal thresholds $I^{nor}_{Crit,V}$ and $I^{nor}_{Crit,NV}$. Using these threshold values, the model could then be spatially extrapolated to delineate wet channels in the associated catchment across a broader area. Data for this representative calibration area could come from ground-based reference observations, a data set such as the NHD, or coincident aerial imagery, depending on availability. For example, Figure 13a depicts a small, randomly selected area from Basin 2, where a perennial stream (Blackwood Creek) can be seen weaving in and out of canopy cover. A probability density analysis of intensity data from this area (Figure 13b) produced an $I^{nor}_{Crit,V}$ value of 0.56, only slightly greater than the result for the whole of Basin 2 ($I^{nor}_{Crit,V} = 0.53$). Therefore, using only this ~0.15 km^2 area for calibration, the model could have been extrapolated over the entire Basin 2 drainage area with comparable results to those presented in Section 4. Alternatively, if no ground truth, imagery, or other reference data is available, a practitioner could utilize Gaussian mixture models, as in Hooshyar et al. (2015). However, as we have demonstrated, data coincident with dense vegetation should be evaluated separately, even with this approach. Last, although spatial extrapolation appears practical when evaluated carefully, it is important to note that temporal extrapolation is likely imprudent, especially over seasonal time scales. Changes in ground cover, the state of vegetation (e.g., pre- vs. post-leaf out), the weather conditions, or the sensor used, for example, could shift optimal thresholds between data acquisitions. This is evident when we compare thresholds between Basin 4M and 4A (Table 2).

The classification workflow demonstrated a median accuracy of 93.0% across all data sets, though with notable strengths and weaknesses. For instance, the model was exceptional at excluding NHD-designated intermittent and ephemeral channels from the wet channel classification during low flow conditions, meaning there were very few

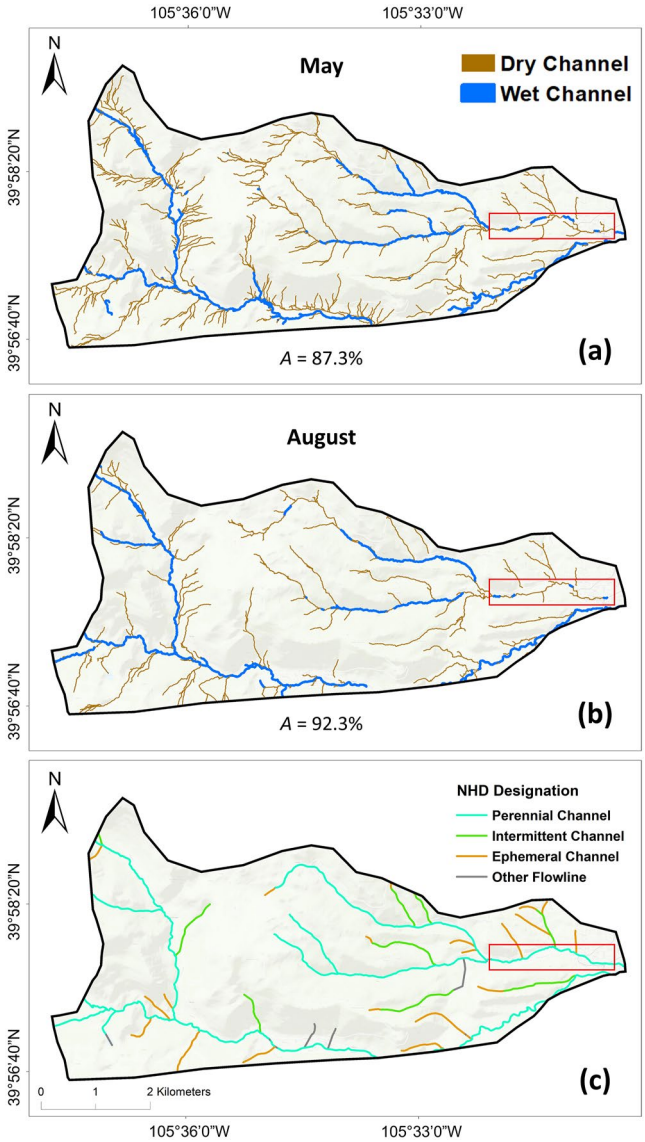

Figure 12. Classified maps depicting the extent of modeled wet and dry channel lengths (a and b) compared temporally and to National Hydrography Dataset channel designations (c) for Basin 4 atop topographic relief. The red rectangle highlights an area where inaccurate spatial drainage delineation caused misclassification.

FPs. However, we qualitatively note that our model misclassifies perennial channels as dry more frequently as proximity to channel heads increases, where stream widths tend to be at a minimum. This likely implies a stream width limitation in our classified product related to lidar ground return point spacing, where an insufficient density of low-intensity pixels results in misclassification. Misclassification near perennial channel heads contributed to our classification workflow's tendency to underestimate wetted channel lengths when compared to the NHD, as noted in Section 4. Model uncertainty can be quantified by the area under probability density curves, as demonstrated in Figure 13b. The area under the blue $I^{nor}_{D,V,Wet}$ curve beyond the critical $I^{nor}_{Crit,V}$ threshold value (highlighted in red) is 0.14. Thus, in this case we would anticipate wet pixels under dense vegetation to be misclassified as dry (hence false negatives, FN) about 14% of the time.

We note that there is a certain degree of unquantifiable uncertainty involved in our validation procedure, namely from the lack of ground truth. Though careful site/data set selection, NHD periodicity classifications, hydrograph, and precipitation data provided an excellent understanding of the hydrologic conditions during lidar data acquisition, it is impossible to know for certain which streams were wet versus dry in the absence of ground-based observations. Simply put, reliance on static NHD permanence designations is an inherent source of uncertainty. Though the NHD is the most comprehensive hydrography data set in the United States, its accuracy continues to evolve and improve. For instance, Hafen et al. (2020) found that it is not uncommon for in situ streamflow observations to disagree with NHD periodicity classifications, and noted the dynamic influence of climate variability on this disagreement. Further, the coarse spatial resolution of NHD periodicity classifications (relative to the 1 m resolution used here) presents a limitation. Complex oscillations between perennial and temporary streams over relatively short spatial scales are frequent in nature, due to localized elevated water tables, for example, Unfortunately, extensive in situ observations are almost never coincident with historical lidar data sets.

It is apparent that smoothing each stream link segment by the majority pixel classification resulted in occasional discontinuity in the wet channel network (Figures 11 and 12). Although perhaps aesthetically unappealing, this discontinuity likely provides useful insight. As mentioned above, disjointed sections may indicate a need to re-evaluate or increase the spatial resolution of stream periodicity assignments. Furthermore, temporary (intermittent and ephemeral) streams oscillate between three main hydrological states: dry, disjointed standing pools, and flowing water, varying seasonally and in response to rainfall/snowmelt events (Assendelft & van Meerveldt, 2019; Buttle et al., 2012). The timing of these dynamics is of great importance to the fields of ecology and biochemistry (Leigh et al., 2016; McClain et al., 2003; Meyer et al., 2007); for example, temporary channels and their associated vegetative communities play a key role as migration corridors (Goodrich et al., 2018). Therefore, disconnected segments may well reflect vital ecological processes. Additionally, temporary stream dynamics reflect subsurface storage patterns (Camporese et al., 2010), affect downstream discharge flow rates (Godsey & Kirchner, 2014), along with water quality and nutrient availability (Romaní et al., 2006). Our model demonstrated its capacity to capture this temporal variation of intermittent channels, as is evident in Basin 4 (Figure 14).

Calculations of intensity reduction in wet channels relative to dry channels were in good agreement with comparable literature. Across drainage basins, we observed an average reduction in median Normalized Intensity of

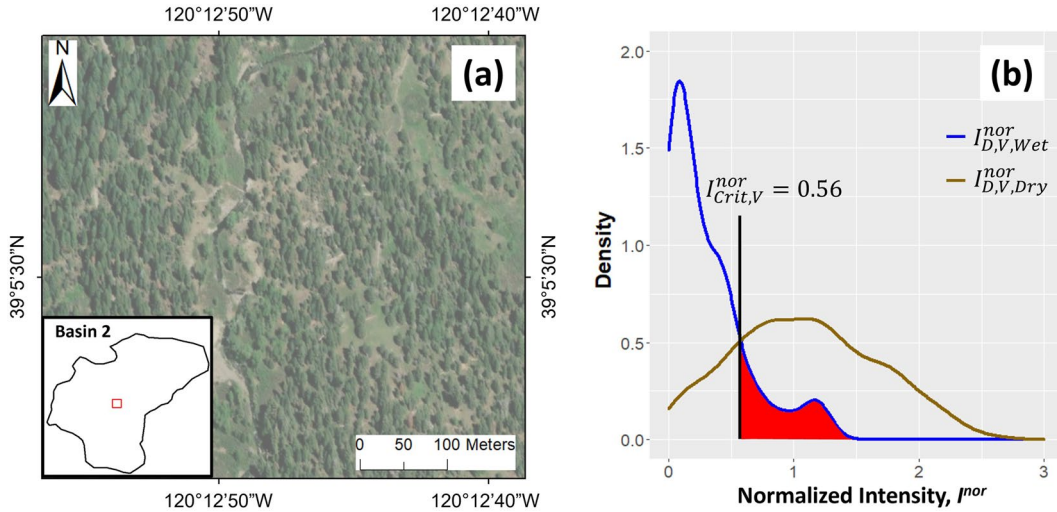

Figure 13. Randomly selected, representative area along Blackwood Creek in Basin 2 (a) used to demonstrate model calibration in practice. Probability density functions from this calibration area (b) produced nearly the same critical threshold as that of the entire basin. The red highlighted area under the curve represents the probability of misclassification, used to quantify model uncertainty.

41.7% under dense vegetation ($I^{nor}_{D,V,Wet}$ vs. $I^{nor}_{D,V,Dry}$) and 72.2% for areas with no dense vegetation ($I^{nor}_{D,NV,Wet}$ vs. $I^{nor}_{D,NV,Dry}$). A smaller reduction in the presence of dense vegetation is to be expected due to the multiple return phenomenon described in Section 1. Song et al. (2002) demonstrated a reduction of about 80%, while Antonarakis et al. (2008) calculated an optimal threshold for water delineation that was 44% less than that of grass and low vegetation. Lang and McCarty (2009), who did encounter considerable canopy cover in portions of their study area while mapping inundated wetlands, recorded a mean reduction of 85%, although they did not segregate pixels under dense vegetation in the manner presented here. Hooshyar et al. (2015), who also focused on narrow channels but masked dense vegetation, found reductions in optimal delineation thresholds between wet and dry channels from 46% to 73%. Therefore, the intensity results calculated here were within the range of values recorded in similar studies. The work presented here represents one of the most thorough statistical analyses of

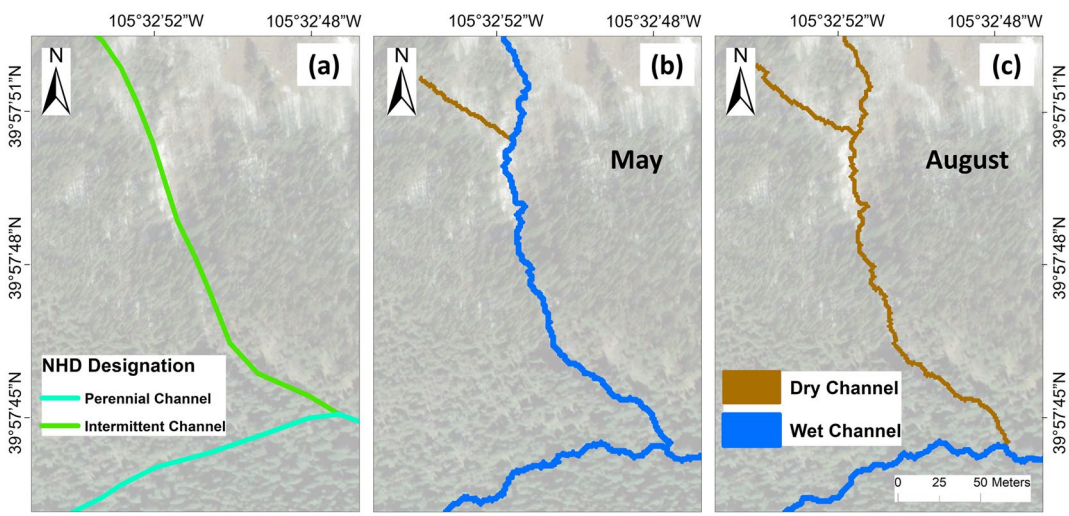

Figure 14. National Hydrography Dataset channel designations (a) compared with classified maps (b and c) depicting an intermittent channel along North Beaver Creek in Basin 4. The channel flows with snowmelt runoff in May as the catchment approaches peak flows (b) then runs dry as the drainage nears baseflow (c).

wet channel intensity reduction to date, and to our knowledge the only study to demonstrate this phenomenon strictly under dense vegetation.

Accuracy of the classified data products were also comparable to that of related research efforts. Classification accuracy in the work presented here ranged from 87.3% to 95.3%, with a median of 93.0%. Seminal studies focusing on large, continuous water bodies without significant vegetation often boast accuracy upwards of 95% (Antonarakis et al., 2008; Höfle et al., 2009), although the problem of headwater channels under dense vegetation is undoubtedly more difficult. Lang and McCarty (2009) performed, to our knowledge, the only other study that focused on intensity signatures under vegetation to map water bodies, though the inundated wetlands in their research area were also large and continuous. They present an impressive accuracy of nearly 97%, however they note a considerable decline in the presence of evergreen forests, such as those in our study sites. Hooshyar et al. (2015), with whom we shared Basins 1–3, did not perform an accuracy assessment and instead centered their validation on correlating estimates of wetted length to streamflow at downstream gages. Qualitatively our results appear comparable. That said, when comparing modeled wet stream channel lengths to NHD reference data (Figure 10) for Basins 1–3, our results demonstrate a mean error of 7.8% while Hooshyar et al. (2015) register 34.7%. In other words, the classified map products presented here are in better agreement with NHD-designated perennial channel lengths during low-flow conditions, the only streams assumed to be flowing as the basins neared baseflow. This improvement indicates the benefit of considering intensity data under dense vegetation rather than excluding it. Therefore, the accuracy of our workflow is on par with similar studies focused only on larger and/or open water bodies, despite confronting the important challenge of small, headwater streams under vegetation.

6. Conclusion and Future Work

We have demonstrated that water under dense vegetation exhibits a distinctly reduced lidar intensity signature compared to dry channels. We then utilized this phenomenon to classify stream networks as wet or dry despite occlusive vegetation. While our findings can be operationalized in their current form, the need for a more complete study is evident. Future studies should combine lidar data acquisition coincident with ground-based data collection to afford more robust reference data than the NHD. Reference data could be acquired manually, or with a ground-based monitoring system like that of Assendelft and van Meerveldt (2019). This would provide an opportunity to better evaluate potential limitations, such as channel width or water depth. Further, the consistency of the observed intensity reduction across varying landscapes should be investigated. In new locations, the statistical significance of differences in wet channel and dry channel intensity under vegetation should be confirmed, as in the work presented here. Geographic factors such as topography, type and extent of vegetation, ground cover, climate, and other parameters will certainly influence the intensity distributions and shift optimal classification thresholds. As lidar data acquisition continues to decrease in expense and increase in frequency, this methodology can be used as a means of remotely mapping occluded wet channel networks and observing temporal dynamics, particularly in challenging landscapes where field observations are difficult. Pairing lidar sensors with unmanned aerial systems, like that of Spence and Mengistu (2016), will assist in achieving sufficient spatial and temporal resolution for the broader implementation of our method.

Appendix A

Relevant statistics for lidar data collection campaigns are listed in Table A1.

Table A1
Summary of Lidar Collection Statistics

Data set	Scanner	Wavelength (nm)	Scan angle	Flight altitude (m)	Point density (points/m^2)	Pulse rate (kHz)
Lake Tahoe Basin	Leica ALS50	1,064	14°	900–1300	13.20	83–106
Boulder Creek Critical Zone Observatory	Optech Gemini	1,047	14°	600	10.28	33–167

Data Availability Statement

Lidar data used in this study were acquired from the public Open Topography repository (https://www.opentopography.org/). NHD data were accessed through the USGS via The National Map interface (https://www.usgs.gov/the-national-map-data-delivery), while stream gage data for Basins 1–3 were also procured from the USGS (https://waterdata.usgs.gov/nwis/rt). Stream gage data for Basin 4 was provided by the Colorado Department of Water Resources (https://dwr.state.co.us/tools/stations). Last, precipitation data were acquired from the National Climate Data Center (https://www.ncdc.noaa.gov/cdo-web/search).

Acknowledgments
The authors would like to thank Dr. Kathryn Plymesser, Dr. Scott Powell, and four anonymous reviewers for their invaluable commentary and insights.

References

Abalharth, M., Hassan, M. A., Klinkenberg, B., Leung, V., & McCleary, R. (2015). Using LiDAR to characterize logjams in lowland rivers. *Geomorphology*, *246*, 531–541. https://doi.org/10.1016/j.geomorph.2015.06.036

Antonarakis, A. S., Richards, K. S., & Brasington, J. (2008). Object-based land cover classification using airborne LiDAR. *Remote Sensing of Environment*, *112*(6), 2988–2998. https://doi.org/10.1016/j.rse.2008.02.004

Assendelft, R. S., & van Meerveld, H. J. (2019). A low-cost, multi-sensor system to monitor temporary stream dynamics in mountainous headwater catchments. *Sensors*, *19*(21), 4645. https://doi.org/10.3390/s19214645

Brzank, A., Heipke, C., Goepfert, J., & Soergel, U. (2008). Aspects of generating precise digital terrain models in the Wadden Sea from lidar–water classification and structure line extraction. *ISPRS Journal of Photogrammetry and Remote Sensing*, *63*(5), 510–528. https://doi.org/10.1016/j.isprsjprs.2008.02.002

Buttle, J. M., Boon, S., Peters, D. L., Spence, C., Van Meerveld, H. J., & Whitfield, P. H. (2012). An overview of temporary stream hydrology in Canada. *Canadian Water Resources Journal/Revue Canadienne Des Ressources Hydriques*, *37*(4), 279–310. https://doi.org/10.4296/cwrj2011-903

Camporese, M., Paniconi, C., Putti, M., & Orlandini, S. (2010). Surface-subsurface flow modeling with path-based runoff routing, boundary condition-based coupling, and assimilation of multisource observation data. *Water Resources Research*, *46*(2). https://doi.org/10.1029/2008wr007536

Colvin, R., Giannico, G. R., Li, J., Boyer, K. L., & Gerth, W. J. (2009). Fish use of intermittent watercourses draining agricultural lands in the Upper Willamette River Valley, Oregon. *Transactions of the American Fisheries Society*, *138*(6), 1302–1313. https://doi.org/10.1577/t08-150.1

Colvin, S. A., Sullivan, S. M. P., Shirey, P. D., Colvin, R. W., Winemiller, K. O., Hughes, R. M., et al. (2019). Headwater streams and wetlands are critical for sustaining fish, fisheries, and ecosystem services. *Fisheries*, *44*(2), 73–91. https://doi.org/10.1002/fsh.10229

Devito, K., Creed, I., Gan, T., Mendoza, C., Petrone, R., Silins, U., & Smerdon, B. (2005). A framework for broad-scale classification of hydrologic response units on the Boreal Plain: Is topography the last thing to consider? *Hydrological Processes: An International Journal*, *19*(8), 1705–1714. https://doi.org/10.1002/hyp.5881

Erman, D. C., & Leidy, G. R. (1975). Downstream movement of rainbow trout fry in a tributary Sagehen Creek, under permanent and intermittent flow. *Transactions of the American Fisheries Society*, *104*(3), 467–473. https://doi.org/10.1577/1548-8659(1975)104<467:dmortf>2.0.co;2

ESRI. (2020). *ArcGIS desktop: Release 10.8.1*. Environmental Systems Research Institute.

Foody, G. M. (2002). Status of land cover classification accuracy assessment. *Remote Sensing of Environment*, *80*(1), 185–201. https://doi.org/10.1016/s0034-4257(01)00295-4

Foody, G. M. (2009). Sample size determination for image classification accuracy assessment and comparison. *International Journal of Remote Sensing*, *30*(20), 5273–5291. https://doi.org/10.1080/01431160903130937

Godsey, S. E., & Kirchner, J. W. (2014). Dynamic, discontinuous stream networks: Hydrologically driven variations in active drainage density, flowing channels and stream order. *Hydrological Processes*, *28*(23), 5791–5803. https://doi.org/10.1002/hyp.10310

Goodrich, D. C., Kepner, W. G., Levick, L. R., & Wigington, P. J., Jr. (2018). Southwestern intermittent and ephemeral stream connectivity. *JAWRA Journal of the American Water Resources Association*, *54*(2), 400–422. https://doi.org/10.1111/1752-1688.12636

Hack, J. T., & Goodlett, J. C. (1960). *Geomorphology and forest ecology of a mountain region in the central Appalachians* (No. 347). United States Government Printing Office.

Hafen, K. C., Blasch, K. W., Rea, A., Sando, R., & Gessler, P. E. (2020). The influence of climate variability on the accuracy of NHD perennial and nonperennial stream classifications. *JAWRA Journal of the American Water Resources Association*, *56*(5), 903–916. https://doi.org/10.1111/1752-1688.12871

Haigh, M. J., Singh, R. B., & Krecek, J. (1998). Headwater control: Matters arising. In M. J. Haigh, J. Krecek, G. S. Rajwar, & M. P. Kilmartin (Eds.), *Headwaters: Water resources and soil conservation* (Vol. 3, p. 24). AA Balkema.

Hartman, G. F., & Brown, T. G. (1987). Use of small, temporary, floodplain tributaries by juvenile salmonids in a west coast rain-forest drainage basin, Carnation Creek, British Columbia. *Canadian Journal of Fisheries and Aquatic Sciences*, *44*(2), 262–270. https://doi.org/10.1139/f87-035

Hay, A. M. (1979). Sampling designs to test land-use map accuracy. *Photogrammetric Engineering and Remote Sensing*, *45*(4), 529–533.

Höfle, B., Vetter, M., Pfeifer, N., Mandlburger, G., & Stötter, J. (2009). Water surface mapping from airborne laser scanning using signal intensity and elevation data. *Earth Surface Processes and Landforms*, *34*(12), 1635–1649. https://doi.org/10.1002/esp.1853

Hooshyar, M., Kim, S., Wang, D., & Medeiros, S. C. (2015). Wet channel network extraction by integrating LiDAR intensity and elevation data. *Water Resources Research*, *51*(12), 10029–10046. https://doi.org/10.1002/2015wr018021

Horton, R. E. (1945). Erosional development of streams and their drainage basins; hydrophysical approach to quantitative morphology. *Geological Society of America Bulletin*, *56*(3), 275–370. https://doi.org/10.1130/0016-7606(1945)56[275:edosat]2.0.co;2

Jacobson, P. M. (2004). *Connecticut River ecological study (1965-1973) revisited*. American Fisheries Society.

James, L. A., & Hunt, K. J. (2010). The LiDAR-side of headwater streams: Mapping channel networks with high-resolution topographic data. *Southeastern Geographer*, *50*(4), 523–539. https://doi.org/10.1353/sgo.2010.0009

James, L. A., Watson, D. G., & Hansen, W. F. (2007). Using LiDAR data to map gullies and headwater streams under forest canopy: South Carolina, USA. *Catena*, *71*(1), 132–144. https://doi.org/10.1016/j.catena.2006.10.010

Lang, M. W., & McCarty, G. W. (2009). Lidar intensity for improved detection of inundation below the forest canopy. *Wetlands*, *29*(4), 1166–1178. https://doi.org/10.1672/08-197.1

Larned, S. T., Datry, T., Arscott, D. B., & Tockner, K. (2010). Emerging concepts in temporary-river ecology. *Freshwater Biology*, *55*(4), 717–738. https://doi.org/10.1111/j.1365-2427.2009.02322.x

Lashermes, B., Foufoula-Georgiou, E., & Dietrich, W. E. (2007). Channel network extraction from high resolution topography using wavelets. *Geophysical Research Letters*, *34*(23). https://doi.org/10.1029/2007gl031140

Leigh, C., Boulton, A. J., Courtwright, J. L., Fritz, K., May, C. L., Walker, R. H., & Datry, T. (2016). Ecological research and management of intermittent rivers: An historical review and future directions. *Freshwater Biology*, *61*(8), 1181–1199. https://doi.org/10.1111/fwb.12646

Leopold, L. B. (1994). *A view of the river*. Harvard University Press.

Leopold, L. B., & Miller, J. P. (1956). *Ephemeral streams: Hydraulic factors and their relation to the drainage net* (Vol. 282). US Government Printing Office.

Leopold, L. B., Wolman, M. G., & Miller, J. P. (1964). *Fluvial processes in geomorphology*. Dover Publications.

McClain, M. E., Boyer, E. W., Dent, C. L., Gergel, S. E., Grimm, N. B., Groffman, P. M., et al. (2003). Biogeochemical hot spots and hot moments at the interface of terrestrial and aquatic ecosystems. *Ecosystems*, *6*(4), 301–312. https://doi.org/10.1007/s10021-003-0161-9

McDonough, O. T., Hosen, J. D., & Palmer, M. A. (2011). Temporary streams: The hydrology, geography, and ecology of non-perennially flowing waters. *River Ecosystems: Dynamics, Management and Conservation*, 259–290.

McFeeters, S. K. (1996). The use of the Normalized Difference Water Index (NDWI) in the delineation of open water features. *International Journal of Remote Sensing*, *17*(7), 1425–1432. https://doi.org/10.1080/01431169608948714

Meyer, J. L., Strayer, D. L., Wallace, J. B., Eggert, S. L., Helfman, G. S., & Leonard, N. E. (2007). The contribution of headwater streams to biodiversity in river networks 1. *JAWRA Journal of the American Water Resources Association*, *43*(1), 86–103. https://doi.org/10.1111/j.1752-1688.2007.00008.x

Meyer, J. L., & Wallace, J. B. (2001). Lost linkages and lotic ecology: Rediscovering small streams. In *Ecology: Achievement and challenge: The 41st symposium of the British Ecological Society sponsored by the Ecological Society of America held at Orlando*, Florida, USA, 10–13 April 2000 (pp. 295–317). Blackwell Science.

Montgomery, D. R. (1999). Process domains and the river continuum 1. *JAWRA Journal of the American Water Resources Association*, *35*(2), 397–410. https://doi.org/10.1111/j.1752-1688.1999.tb03598.x

Nadeau, T. L., & Rains, M. C. (2007). Hydrological connectivity between headwater streams and downstream waters: How science can inform policy 1. *JAWRA Journal of the American Water Resources Association*, *43*(1), 118–133. https://doi.org/10.1111/j.1752-1688.2007.00010.x

Omran, A., Dietrich, S., Abouelmagd, A., & Michael, M. (2016). New ArcGIS tools developed for stream network extraction and basin delineations using Python and java script. *Computers & Geosciences*, *94*, 140–149. https://doi.org/10.1016/j.cageo.2016.06.012

Orlandini, S., Tarolli, P., Moretti, G., & Dalla Fontana, G. (2011). On the prediction of channel heads in a complex alpine terrain using gridded elevation data. *Water Resources Research*, *47*(2). https://doi.org/10.1029/2010wr009648

Passalacqua, P., Do Trung, T., Foufoula-Georgiou, E., Sapiro, G., & Dietrich, W. E. (2010). A geometric framework for channel network extraction from lidar: Nonlinear diffusion and geodesic paths. *Journal of Geophysical Research*, *115*(F1), F01002. https://doi.org/10.1029/2009jf001254

R Core Team. (2022). *R: A language and environment for statistical computing*. R Foundation for Statistical Computing. Retrieved from https://www.R-project.org/

Romaní, A. M., Vázquez, E., & Butturini, A. (2006). Microbial availability and size fractionation of dissolved organic carbon after drought in an intermittent stream: Biogeochemical link across the stream–riparian interface. *Microbial Ecology*, *52*(3), 501–512. https://doi.org/10.1007/s00248-006-9112-2

Simley, J. (2006). The national hydrography dataset: Introduction. *Water Resources IMPACT*, *8*(2), 4.

Song, J. H., Han, S. H., Yu, K. Y., & Kim, Y. I. (2002). Assessing the possibility of land-cover classification using lidar intensity data. *The International Archives of the Photogrammetry, Remote Sensing and Spatial Information Sciences*, *34*(3/B), 259–262.

Spence, C., & Mengistu, S. (2016). Deployment of an unmanned aerial system to assist in mapping an intermittent stream. *Hydrological Processes*, *30*(3), 493–500. https://doi.org/10.1002/hyp.10597

Stehr, W. C., & Branson, J. W. (1938). An ecological study of an intermittent stream. *Ecology*, *19*(2), 294–310. https://doi.org/10.2307/1929643

Story, M., & Congalton, R. G. (1986). Accuracy assessment: A user's perspective. *Photogrammetric Engineering & Remote Sensing*, *52*(3), 397–399.

Tennant, D. L. (1976). Instream flow regimens for fish, wildlife, recreation and related environmental resources. *Fisheries*, *1*(4), 6–10. https://doi.org/10.1577/1548-8446(1976)001<0006:ifrffw>2.0.co;2

Uys, M. C., & O'Keeffe, J. H. (1997). Simple words and fuzzy zones: Early directions for temporary river research in South Africa. *Environmental Management*, *21*(4), 517–531. https://doi.org/10.1007/s002679900047

Wipfli, M. S., Richardson, J. S., & Naiman, R. J. (2007). Ecological linkages between headwaters and downstream ecosystems: Transport of organic matter, invertebrates, and wood down headwater channels 1. *JAWRA Journal of the American Water Resources Association*, *43*(1), 72–85. https://doi.org/10.1111/j.1752-1688.2007.00007.x

Work, E. A., & Gilmer, D. S. (1976). Utilization of satellite data for inventorying prairie ponds and lakes. *Photogrammetric Engineering and Remote Sensing*, *42*(5), 685–694.

Worstell, B. B., Poppenga, S., Evans, G. A., & Prince, S. (2014). *Lidar point density analysis: Implications for identifying water bodies*. US Geological Survey.

Xu, H. (2006). Modification of normalised difference water index (NDWI) to enhance open water features in remotely sensed imagery. *International Journal of Remote Sensing*, *27*(14), 3025–3033. https://doi.org/10.1080/01431160600589179